Intrinsic functional architecture predicts electrically evoked responses in the human brain

Corey J. Keller[a,1], Stephan Bickel[b,c,d,1], László Entz[c,d,e,f], Istvan Ulbert[e,f,g], Michael P. Milham[h,i], Clare Kelly[h], and Ashesh D. Mehta[b,c,d,2]

[a]Albert Einstein College of Medicine, Bronx, NY 10461; Departments of [b]Neurology and [c]Neurosurgery, North Shore Long Island Jewish Health System, and [d]Feinstein Institute for Medical Research, Hofstra University School of Medicine, Manhasset, NY 11030; [e]Institute for Psychology of the Hungarian Academy of Sciences, Budapest 1068, Hungary; [f]National Institute of Neuroscience, Budapest, Hungary; [g]Faculty of Information Technology, Péter Pázmány Catholic University, Budapest, Hungary; [h]Phyllis Green and Randolph Cowen Institute for Pediatric Neuroscience, New York University Child Study Center, New York, NY 10016; and [i]Nathan Kline Institute for Psychiatric Research, Orangeburg, NY 10962

Edited by Marcus E. Raichle, Washington University of St. Louis, St. Louis, MO, and approved April 27, 2011 (received for review January 8, 2011)

Adaptive brain function is characterized by dynamic interactions within and between neuronal circuits, often occurring at the time scale of milliseconds. These complex interactions between adjacent and noncontiguous brain areas depend on a functional architecture that is maintained even in the absence of input. Functional MRI studies carried out during rest (R-fMRI) suggest that this architecture is represented in low-frequency (<0.1 Hz) spontaneous fluctuations in the blood oxygen level-dependent signal that are correlated within spatially distributed networks of brain areas. These networks, collectively referred to as the brain's intrinsic functional architecture, exhibit a remarkable correspondence with patterns of task-evoked coactivation as well as maps of anatomical connectivity. Despite this striking correspondence, there is no direct evidence that this intrinsic architecture forms the scaffold that gives rise to faster processes relevant to information processing and seizure spread. Here, we demonstrate that the spatial distribution and magnitude of temporally correlated low-frequency fluctuations observed with R-fMRI during rest predict the pattern and magnitude of corticocortical evoked potentials elicited within 500 ms after single-pulse electrical stimulation of the cerebral cortex with intracranial electrodes. Across individuals, this relationship was found to be independent of the specific regions and functional systems probed. Our findings bridge the immense divide between the temporal resolutions of these distinct measures of brain function and provide strong support for the idea that the low-frequency signal fluctuations observed with R-fMRI maintain and update the intrinsic architecture underlying the brain's repertoire of functional responses.

functional connectivity | resting state

There is mounting evidence that the temporally correlated low-frequency fluctuations that engender the brain's intrinsic functional architecture are relevant to brain function. Studies relating variation within this intrinsic architecture to behavior, cognition, psychopathology, and neurological disease have captured the attention of the neuroscientific, psychological, and clinical communities alike (1–4). Despite early controversies regarding the origins of the blood oxygen level-dependent (BOLD) signal fluctuations commonly used to map the intrinsic architecture, recent work demonstrating their electrophysiological correlates suggests a neural origin (5–8). However, the neurophysiological significance of correlated brain activity occurring on such slow time scales remains elusive. Emerging hypotheses suggest a role for this slow activity in the maintenance and reinforcement of the synaptic connections that support cognition and action (9, 10). Central to this suggestion is the assumption that corticocortical dynamics that take place over faster time scales are embedded in its intrinsic functional architecture; however, no direct evidence of this exists to date.

By electrically stimulating the cerebral cortex via intracranial electrodes implanted in patients with intractable seizures, we can directly relate electrical activity occurring over rapid time scales to the same individual's intrinsic functional architecture, previously mapped using resting state functional MRI (R-fMRI) data. Here, we use this approach to test the hypothesis that the spatial distribution and magnitude of evoked neuronal activity are predicted by the pattern and strength of temporal correlations among the spontaneous BOLD fluctuations exhibited by spatially distinct regions, commonly referred to as resting state functional connectivity (RSFC). Specifically, we predicted that (*i*) the spatial distribution of the electrical response to direct stimulation [i.e., corticocortical evoked potential (CCEP)] would follow that of the intrinsic functional architecture (i.e., RSFC) associated with the stimulated site and (*ii*) regions within the architecture exhibiting the strongest RSFC with the stimulated site would show the highest magnitude electrically evoked responses.

Results

For each of six patients with intractable epilepsy, we investigated the relationship between RSFC and CCEPs. CCEPs are elicited in response to single-pulse electrical stimulation of the cortex, with subdural electrodes implanted for the purpose of seizure localization (clinical information and demographics are presented in *SI* Table S1). CCEPs permit us to "electrically track" corticocortical neuronal connections in vivo by stimulating one cortical region and recording the evoked potentials at another location, because responses at the recorded site are the direct result of neuronal projections from the stimulation site (11–13). To obtain CCEPs, we administered repeated brief single-pulse electrical currents between adjacent electrodes and recorded the evoked electrophysiological responses at all other implanted electrode sites (Fig. 1*A*). This procedure was repeated for all possible adjacent stimulation sites. To derive RSFC maps, we first localized the implanted electrodes via coregistration with the patient's anatomical MRI and computed tomography (CT) scans (*Materials and Methods*). The obtained coordinates formed the centers of spherical regions of interest (ROIs) ("seeds"), and the temporal correlation (RSFC) between each seed's mean time series and the BOLD signal at every other voxel in the brain was then calculated (Fig. 1*B*). The fMRI scan was acquired before electrode implantation.

For each stimulation site, we first computed the correlation between CCEP amplitudes and RSFC values at each electrode

Author contributions: S.B., L.E., I.U., and A.D.M. designed research; S.B., L.E., and A.D.M. performed experiments; C.J.K., S.B., and L.E. analyzed data; and C.J.K., S.B., L.E., I.U., M.P.M., C.K., and A.D.M. wrote the paper.

The authors declare no conflict of interest.

This article is a PNAS Direct Submission.

Data deposition: The resting state fMRI data used to prepare this manuscript are available to the public through the International Neuroimaging Data-sharing Initiative (INDI), by visiting the link http://fcon_1000.projects.nitrc.org/.

[1]C.J.K. and S.B. contributed equally to this work.

[2]To whom correspondence should be addressed. E-mail: amehta@nshs.edu.

This article contains supporting information online at www.pnas.org/lookup/suppl/doi:10.1073/pnas.1019750108/-/DCSupplemental.

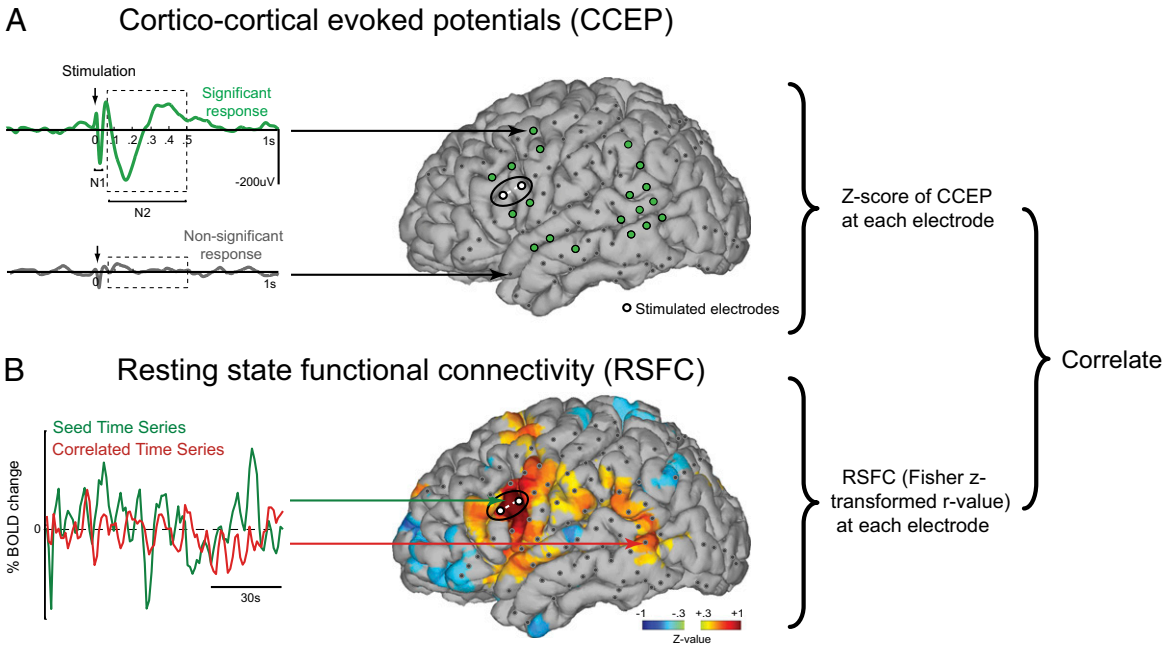

Fig. 1. Analysis schematic. (*A*) CCEPs in response to single-pulse electrical stimulation of each electrode pair were recorded at all implanted electrodes. Responses were categorized as significant or nonsignificant if the average waveform exceeded a statistical threshold of 6 SDs during an interval of 50–500 ms poststimulation. For visualization purposes, the locations of significant responses were overlaid onto the individual's reconstructed pial surface. The magnitude of CCEPs at each electrode was computed as a *z* score relative to baseline of each stimulation site. (*B*) RSFC maps associated with spherical ROIs underlying the stimulated electrodes were computed for each stimulation site. For visualization, the RSFC maps were displayed on the reconstructed pial surface. To examine the correlation between RSFC and CCEP values, Fisher's *z*-transformed correlation coefficients were extracted from the voxels underlying each electrode and correlated with the CCEPs recorded from the same electrodes. The schematic shows data from Subject 1 as an illustration.

without applying any thresholding to either RSFC or the CCEPs (i.e., all values were included in the analysis; Fig. 2*C*). The mean relationship across all stimulation sites was significant in each individual subject [S1: $t(44) = 37.9$, $P < 0.001$; S2: $t(15) = 36.7$, $P < 0.001$; S3: $t(39) = 26.5$, $P < 0.001$; S4: $t(35) = 23.9$, $P < 0.001$; S5: $t(20) = 41.9$, $P < 0.001$; S6: $t(25) = 53.4$, $P < 0.001$] as well as across all six subjects [$t(5) = 21.4$; $P < 0.001$], indicating that the relationship between RSFC values and CCEP amplitudes was independent of the stimulated brain area. Next, we computed a binary response matrix for each stimulation site by identifying the electrodes that exhibited a significant CCEP (details of CCEP thresholding are presented in *Materials and Methods* and Fig. S1). In all but one patient, electrodes exhibiting a significant CCEP demonstrated higher RSFC than those that did not exhibit a significant CCEP ($P < 0.05$; Fig. 2*A*). When this analysis was repeated for the P1 and N1 time windows, the same pattern of results was observed (Fig. S2). As is to be expected, the strongest CCEPs and RSFC were observed in electrodes proximal to the stimulation (seed) site. To rule out the possibility that the CCEP/RSFC relationship is based only on local properties, we repeated the comparison between RSFC and CCEPs, excluding electrodes within 25 mm of the stimulation site. Although RSFC decreased overall, correlations between CCEPs and RSFC remained significant ($P < 0.05$; Fig. 2*B*). Additionally, regression analysis demonstrated that the CCEP/RSFC relationship remained highly significant after the effect of distance was removed from both CCEP responses and RSFC values by regression (Fig. S3).

To assess the correspondence between the spatial distribution of significant CCEPs and RSFC over established functional networks, electrodes overlying expressive and nonexpressive language areas as well as hand motor areas were identified using electrical stimulation mapping (ESM; see *Materials and Methods*). For each of these identified electrodes, maps of significant CCEPs and RSFC were calculated and overlaid onto the brain surface (Fig. 3). Each figure shows the tight correspondence between spatial distributions of the CCEP and RSFC maps associated with those electrodes. The spatial correspondence is perhaps most impressive for networks associated with expressive (Fig. 3*A*) and nonexpressive (Fig. 3*B*) language regions, because both CCEPs and RSFC elicited reciprocal networks of language areas, including ventrolateral prefrontal cortex, inferior lateral parietal and temporoparietal cortex, and superior and middle temporal cortex, in line with previous studies (14, 15). Similarly, seeds placed in the hand motor area were associated with significant RSFC across adjacent primary and secondary motor and somatosensory areas, premotor cortex, and more distal posterior parietal and lateral prefrontal regions (Fig. 3*C*), also consistent with previous studies (16, 17).

As shown in Fig. 3, a number of regions exhibited negative RSFC with the seed location (i.e., their spontaneous BOLD activity was negatively correlated with that of the seed location). To assess the relationship between negative correlations ("anticorrelations") and CCEPs, we compared CCEP magnitude at sites associated with strong positive, strong negative, and nonsignificant (values centered around zero) RSFC (Fig. 4 *B* and *C*). ANOVA indicated a significant main effect of connectivity type (i.e., positive, negative, nonsignificant) for each individual subject, as well as across subjects [$F(2, 29{,}990) = 338$, $P < 0.001$; Fig. 4*C*]. However, this main effect was primarily driven by the difference between the mean CCEP *z* score at sites associated with positive RSFC and the mean CCEP *z* score at sites associated with negative or nonsignificant RSFC ($P_{\text{pos-nonsig}} < 0.001$, $P_{\text{pos-neg}} < 0.001$). In all subjects, sites associated with positive RSFC exhibited larger CCEP responses than sites associated with either negative or nonsignificant RSFC (Fig. 4*C* and Fig. S4). Across subjects, the mean CCEP response of sites associated with negative RSFC did not differ with that of sites associated with nonsignificant RSFC ($P_{\text{nonsig-neg}} = 0.09$). Within subjects, the direction of differences between sites associated with negative

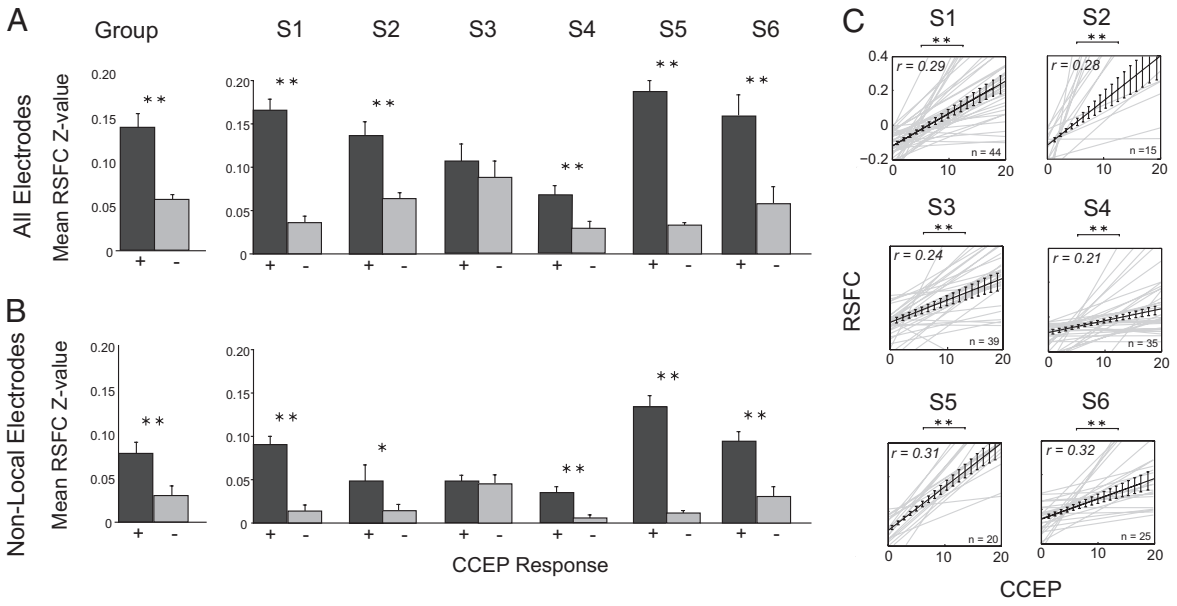

Fig. 2. Relationships between CCEPs and RSFC. (*A*) Group and single-subject analysis. Across all stimulation stites, electrodes exhibiting significant CCEPs (+, dark gray bars) also exhibited significantly higher RSFC *z* values than electrodes exhibiting nonsignificant CCEPs (–, light gray bars), at the group level $t(5) = 9.3$, $P < 0.001$, two-tailed *t* test), and in all but one of the six individual subjects (S1–S6; $*P < 0.05$; $**P < 0.01$). (*B*) Exclusion of proximal electrodes. Significantly higher RSFC *z* values were still observed at electrodes exhibiting significant CCEPs after excluding electrodes within 2.5 cm of the stimulation site ($P < 0.001$, two-tailed *t* test). (*C*) Correlation between RSFC and CCEPs. We computed the correlation between CCEP amplitude and RSFC, across all electrodes, for each stimulation/seed site in each subject, regardless of whether a significant CCEP response was observed (gray lines). Two-tailed *t* tests indicated that the mean relationship across all sites (black line) was significant in each subject (all $P < 0.001$) as well as across all six subjects [$t(5) = 21.4$, $P < 0.001$]. By including all electrodes, this correlation is independent of a priori assumptions implied by amplitude thresholding. The mean *r*-correlation value of all trend lines is reported for each subject (*n* = number of trend lines = number of stimulation sites). CCEPs are reported as *z* scores, and RSFC is reported as a Fisher's *z* value.

RSFC and sites associated with nonsignificant RSFC was inconsistent. Specifically, two of six subjects demonstrated significantly smaller CCEP responses at sites associated with negative correlations than at sites associated with nonsignificant RSFC, whereas one of six showed the opposite pattern and three of six showed no difference (Fig. 4*C*). We repeated this analysis using different methods for defining the positive, negative, and nonsignificant RSFC bins, without appreciable changes in the pattern of results.

Discussion

Patients undergoing electrode implantation surgery for epilepsy are an important population who provide us with a unique invasive window into brain function, by which noninvasive measures may be validated and understood in greater detail (18). Several previous studies have demonstrated strong similarities between the structure of temporal correlations among low-frequency BOLD R-fMRI fluctuations and aspects of the electrocorticography (ECoG) signal recorded from patients with implanted intracranial electrodes. Specifically, similarly correlated slow fluctuations have been observed in neuronal firing rates and in the power of local field potentials in the γ-range (40–100 Hz) as well as in lower frequency ranges (<4 Hz) (5, 9).

Here, we used CCEP mapping, a less conventional and very different method of probing neuronal activity in vivo, to obtain a direct measure of neuronal connectivity and dynamics. Using this method, we demonstrated that the spatial pattern and magnitude of evoked activity in response to direct cortical stimulation were predicted by the pattern and strength of correlations among low-frequency BOLD signal fluctuations. Although epilepsy is likely to have imparted some abnormal properties to the brains of our participants, it is important to note that we demonstrated significant relationships between RSFC and CCEPs in each of six individual participants, all of whom had different forms of focal epilepsy, as well as across the entire group of six subjects.

The neurophysiological underpinnings and functional significance of negative correlations (anticorrelations) in the low-frequency BOLD signal remain subjects of debate (7, 19, 20). Negative connectivity is typically observed between regions or functional systems that appear to subserve competing processes or functions (21, 22). This has led several authors to posit that anticorrelated spatiotemporal activity may be a means of segregating the processing and/or output of these regions (22) or a means of maintaining a dynamic state of readiness that facilitates an efficient response to stimulation (23, 24). Alternatively, it has been argued that negative RSFC is unlikely to have a meaningful neurophysiological basis because it reflects a shift of nonsignificant correlations to the negative range that is a direct result of global signal regression during preprocessing (20). The present work clearly differentiated regions exhibiting positive and negative RSFC in terms of electrophysiological responses. However, analyses were inconclusive with respect to differences in CCEP response amplitude between negatively connected regions and those exhibiting nonsignificant RSFC, suggesting against a simple linear relationship between RSFC and CCEP response amplitude. A better understanding of the functional significance of negative RSFC will likely require targeted examinations that are beyond the scope of the present study, such as time-frequency analyses aimed at understanding whether there are differences between electrodes associated with positive and negative or negative and nonsignificant RSFC in terms of the temporal signature of the responses elicited by electrical stimulation.

Our findings provide strong empirical support for the idea that correlated slow BOLD signal fluctuations provide an intrinsic representation of the brain's repertoire of functional responses (14, 25–28). Future work will benefit from the in-

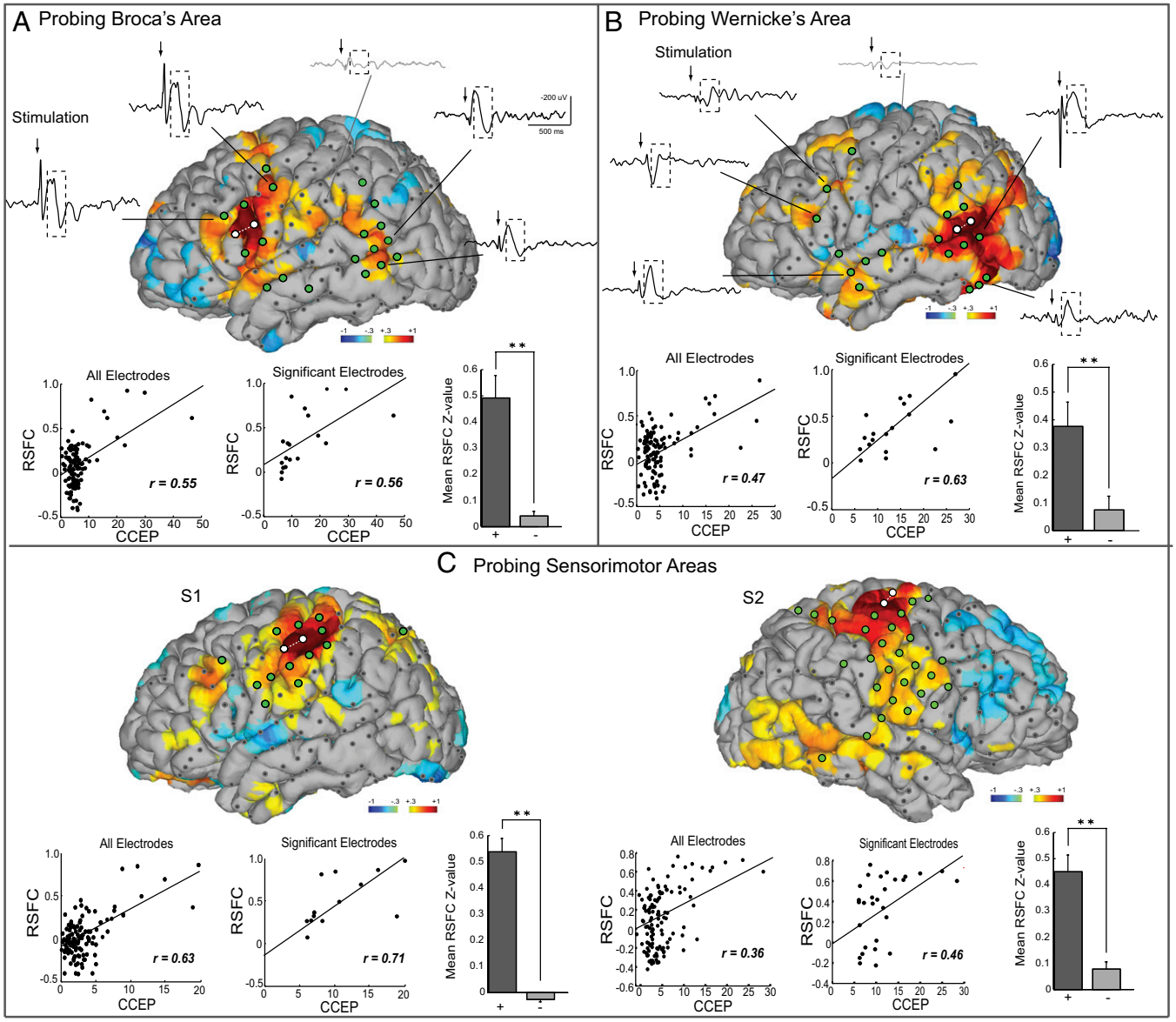

Fig. 3. Probing Broca's area (*A*) and Wernicke's area (*B*) in one patient (S1). Patterns of CCEPs and RSFC are overlaid onto subjects' pial surfaces. Selected significant (black lines) and nonsignificant (gray lines) evoked potentials are shown. The dotted boxes designate the area of interest for determining the significance of the evoked potential (corresponding to the N2 phase). Significant CCEPs (green circles) were observed in close proximity to the stimulation site (e.g., Broca's area) but also in spatially distal areas (e.g., posterior middle and superior temporal cortex). The gray dots indicate electrodes with nonsignificant CCEPs. Areas exhibiting significant RSFC with the seed ROI underlying the stimulation site are shown in yellow/red (positive RSFC) and blue (negative RSFC). Note the striking overlap of electrodes exhibiting significant CCEPs and regions exhibiting significant RSFC. The scatter plots show the relationship between the RSFC Fisher's *z* values and CCEP *z* scores for all recorded electrodes (*Left*) and for electrodes that exhibited significant CCEPs (*Right*). The bar graphs show the mean RSFC *z* values for significant (black) and nonsignificant CCEP electrodes [$P < 0.001$]. (*C*) Probing sensorimotor areas. The remarkable overlap between patterns of RSFC and CCEPs was also observed using seeds and stimulation sites in sensorimotor areas. Examples from two subjects (S1 and S2) are shown. CCEPs are reported as *z* scores, and RSFC is reported as a *z*-correlation value.

tegration of diffusion imaging-based measurement of underlying white matter connectivity, which provides the structural foundation on which the functional architecture is built. The integration of such information will allow us to constrain prediction to those connections shown to be linked by a white matter tract, and will thus likely demonstrate even better correspondence between the intrinsic architecture and evoked responses. Finally, the present findings suggest that R-fMRI approaches may provide a noninvasive alternative to more traditional invasive measures to map spatially distributed networks underlying brain function and pathological networks underlying seizure spread clinically.

Materials and Methods

Patient Selection. Seven patients (four female, aged 35.8 ± 13.4 y, age range: 17–47 y) with pharmacoresistant epilepsy at Long Island Jewish Medical Center participated. All patients provided fully informed consent according to National Institutes of Health guidelines, as monitored by the local institutional review board, in accordance with the ethical standards of the Declaration of Helsinki. Patient characteristics are described in Table S1. Those with overtly abnormal brains, including extensive cortical dysplasias, tumors with vasogenic edema, and strokes, were excluded from this study. One patient was excluded because of difficulty in obtaining reliable CCEPs. ECoG recordings were made over the course of clinical monitoring for spontaneous seizures. The decision to implant, the electrode targets, and the duration of implantation were determined entirely on clinical grounds

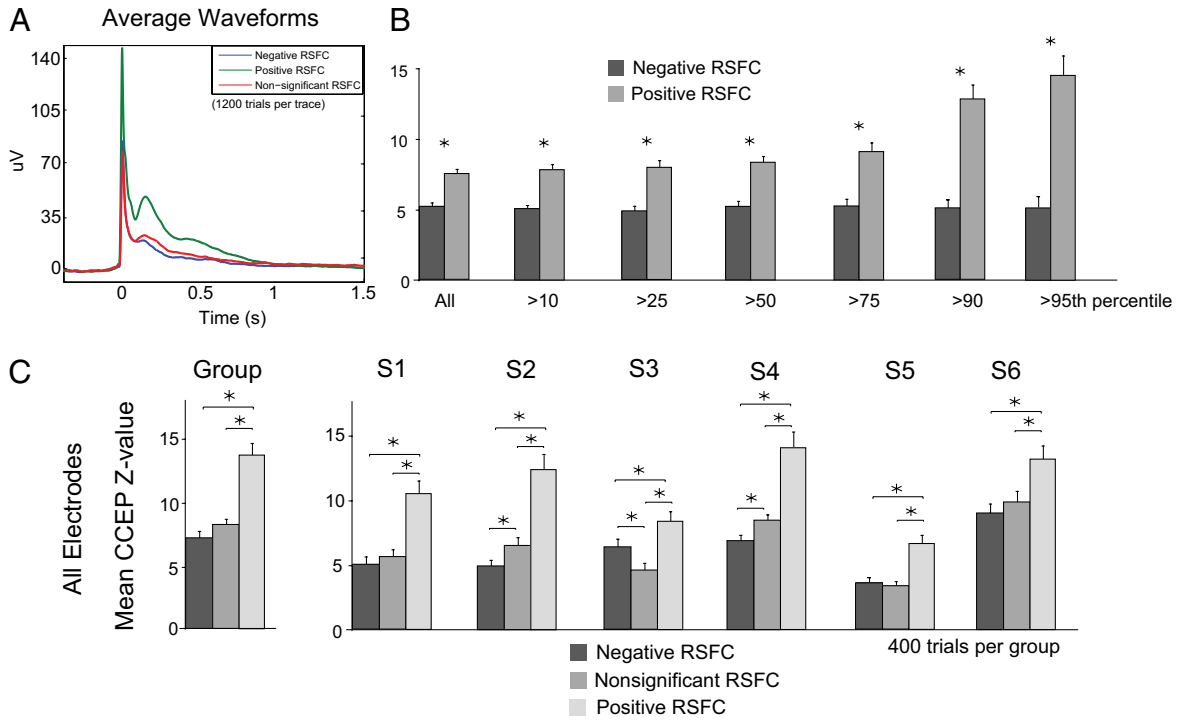

Fig. 4. Negative RSFC correlations. (*A*) CCEP responses were grouped according to whether they were observed at electrode sites exhibiting negative RSFC (400 most negative RSFC values), nonsignificant RSFC (400 RSFC values centered at 0), or positive RSFC (400 most positive RSFC values). Averaged full-wave rectified waveforms are plotted for each group. (*B*) Peak CCEPs for negative and positive RSFC in the N2 time range was calculated using different percentile groups. Although CCEP amplitude increased with increasing positive RSFC values (*$P < 0.01$), no change in CCEP amplitude was observed at sites exhibiting negative RSFC. (*C*) Mean CCEPs were calculated for each RSFC group and each subject (S1–S6). CCEP *z* scores were consistently higher for the positive RSFC group than for the nonsignificant and negative RSFC groups. There was no consistent difference between mean CCEP magnitude for the negative and nonsignificant RSFC groups across subjects.

without reference to this investigation. The patients were informed that participation in this study would not alter their clinical treatment in any way and that they could withdraw at any time without jeopardizing their clinical care.

Cortical Electrical Stimulation for CCEPs. Following implantation of intracranial electrodes, patients were monitored for epileptic activity. During this time, CCEP mapping was performed using single-pulse stimulation. Systematic bipolar stimulation of each pair of adjacent electrodes was administered with single pulses of electrical current (10 mA, 0.5 Hz, 0.2-ms pulse width, 20 trials per electrode pair) using a Grass S12 cortical stimulator (Grass Technologies, Inc.). The associated evoked responses (CCEPs) were measured at all other electrode sites. The current amplitude of 10 mA activated the maximal number of neuronal elements without inducing epileptic afterdischarges or other clinical signs. An interstimulation interval of 2 s was used to minimize the effect of overlapping evoked responses and to leave enough restitution time for the cortex. The stimulation was performed extraoperatively 5 days, on average after electrode implantation surgery, after seizures had been recorded and antiepileptic medications had been resumed. Patients were awake and at rest at the time of CCEP recording.

Functional Stimulation Mapping. For localization of functional cortical areas, ESM was carried out according to standard clinical protocol (bipolar stimulation: 2–5 s, 3–15 mA, 20–50 Hz). Areas were defined as expressive language sites when stimulation resulted in speech arrest. When stimulation resulted in a naming deficit based on auditory or visual cues, or an interruption in reading or comprehension, the area was deemed a nonexpressive language site. Sensory and motor areas were identified when stimulation caused movement or changes in sensation.

Analysis of CCEPs. Electrophysiological data analyses were performed using Neuroscan Edit 4.3 software (Compumedics) and custom MATLAB scripts. Evoked responses to stimulation were divided into 2-s epochs (500 ms prestimulation to 1,500 ms poststimulation) time-locked to stimulation pulse delivery. The early CCEP consists of two major deflections (usually negative in polarity) termed N1 and N2, peaking at ~20–30 ms and 120 ms, respectively. Previous studies showed that the N2 potential exhibits a broader spatial distribution than the N1 potential and occurs between 70 and 300 ms (13). To quantify the magnitude of the CCEPs in the time window of the N2, the data were low-pass filtered (30 Hz), and baseline correction (−500 to −50 ms) was performed. The absolute of the peak *z* score of the response between 50 and 500 ms was then computed using the SD of the baseline. The SD was computed for each electrode separately using all time points in the baseline window of the averaged signal. CCEPs were considered significant if the N2 peak of the evoked potential exceeded the baseline amplitude by a threshold of ±6 SD as determined from the receiver operating characteristic (ROC) curves. For comparison, we also computed CCEPs for the P1 (20–50 ms) and N1 (20–50 ms) time windows, and found similar results (Fig. S5). Evoked responses exceeding ±500 μV were excluded because these most likely indicate electrical artifacts. Responses were color-coded according to significance and plotted on the coregistered cortical pial surface.

Determination of Amplitude Threshold of CCEPs. Direct stimulation on the cortex evokes large responses; therefore, it is not ideal to use conventional statistical thresholds to quantify significance. We relied on a well-established intracortical pathway to calculate a ROC curve to determine the optimal threshold for significance of the evoked response. It is well known that neuroanatomical (29, 30) and functional connections (14, 15) exist between Broca's area and Wernicke's area and that stimulation of Broca's area evokes CCEPs in Wernicke's area (13). To both validate our technique and calculate the threshold response, we stimulated Broca's area and examined the evoked responses in Wernicke's area in the subjects with electrode coverage in language areas. Sensitivity and specificity were calculated based on the evoked response with reference to clinical findings from ESM. True-positives were those electrodes with CCEPs above the threshold and exhibiting a response during functional mapping (e.g., speech arrest). False-positives were those electrodes with CCEPs that were above threshold but at which electrical stimulation had no effect. An optimal threshold showing the best tradeoff between sensitivity and specificity was found at 6 SDs from baseline. This threshold was subsequently used for the duration of the

study (Fig. S1). The correlation analysis was repeated with other thresholds (2–14 SDs), none of which altered results significantly.

Imaging. Patients were scanned on a General Electric Signa HDx 3-T scanner. R-fMRI data were acquired using an echoplanar imaging gradient echo sequence [field of view (FOV) = 220 mm, 3.5 × 3.5 × 4 mm voxel size, 64 × 64 matrix, flip angle = 70, repetition time (TR) = 2,000 ms, echo time (TE) = 30 ms, axial acquisition plane, 150 contiguous volumes]. Participants were instructed to rest with their eyes closed. An anatomical T1-weighted image was acquired using a spoiled gradient recalled sequence [FOV = 256 mm, 1 × 1 × 1 mm voxel size, 256 × 256 matrix, flip angle = 8, TR = 2,500 ms, TE = 30 ms, inversion time = 650 ms, axial acquisition plane, 180 slices].

RSFC. Resting state data preprocessing was performed using AFNI (31) and FSL (32) and included slice timing correction for interleaved slice acquisition, motion correction, despiking, spatial smoothing (6-mm full-width at half-maximum Gaussian blur), band-pass filtering (0.009–0.1 Hz), and linear and quadratic detrending. To remove variance associated with processes such as breathing, cardiac activity and motion, we regressed each patient's preprocessed time series on nine nuisance covariates (six head motion parameters, signals derived from the ventricles and white matter, and global signal). The resultant 4D residuals volume was registered to the patient's anatomical image using a linear transformation with 6 df.

For each patient, and each stimulation site, spherical seed ROIs (6-mm radius) were constructed centered at each electrode. The mean time course for the seed was computed by averaging across all voxels within the seed. A whole-brain map of RSFC was created by computing the correlation between the seed time course and that of every other voxel in the brain and then applying Fisher's *r*-to-*z* transformation to the resultant correlation coefficients. The resultant RSFC map was projected from a 3D volume to the individual's pial surface and plotted using MATLAB, employing a conservative threshold of $z \geq 0.3$ for visualization purposes only (33, 34).

Correspondence Between CCEPs and RSFC. To quantify the correspondence between CCEPs and RSFC, for each stimulation site, we computed the correlation between CCEP *z* scores at each electrode site and Fisher's *z*-transformed correlation (RSFC) values at each corresponding electrode site. The resultant correlations were transformed to *z* values using Fisher's *r*-to-*z* transformation. The statistical significance of the relationship between CCEP *z* scores and RSFC was then assessed for each subject using a two-tailed *t* test (against zero) on the *z*-transformed correlation values. We also assessed the statistical significance of the correlation between CCEP *z* scores and RSFC at the group level by computing the mean (*z*-transformed) correlation (across all stimulation sites) for each subject and entering the resultant values into a two-tailed *t* test (against zero). No thresholding was applied to either RSFC or CCEP values for this analysis (i.e., all values were included in the analysis; Fig. 2*C*).

In a second statistical analysis, we compared the mean RSFC across the electrodes sites that exhibited a significant CCEP response (±6 SD from baseline) with those exhibiting a nonsignificant CCEP response using a two-tailed *t* test. To rule out the possibility that the differences between RSFC at significant and nonsignificant electrodes were driven primarily by electrodes proximal to the stimulation site, this analysis was repeated excluding those electrodes located within 25 mm of the stimulation site (Fig. 2 *A* and *B*).

Negative Correlation RSFC Analysis. To explore the relationship between CCEPs and negative RSFC correlations, we first sorted electrode locations based on whether they exhibited negative, nonsignificant, or positive RSFC with the seed (stimulated) electrode. Next, for each subject, we identified the 400 locations (corresponding to 5–10% of the total CCEPs, depending on the subject) that exhibited the most strongly positive RSFC, the most strongly negative RSFC, and CCEPs with RSFC centered at 0. We then tested for statistically significant differences in the mean CCEP magnitude (i.e., *z* score) across the electrodes in each bin using a one-way ANOVA, followed by two-tailed *t* tests comparing all bins (Fig. 4 *B* and *C*). We repeated this analysis using several different bin sizes (100–1,600) without appreciable changes in the pattern of results.

ACKNOWLEDGMENTS. We thank G. Klein, M. Argyelan, and A. Dykstra for help with developing methodology to coregister electrode location with noninvasive data. F. Lado provided invaluable comments during the preparation of the manuscript. We are enormously indebted to the patients who participated in this study and the nursing and physician staff North Shore Long Island Jewish Medical Center. This work was funded by a grant from the Otto and Page Marx Foundation (to A.M.), Grant K81357 from the OTKA, and a grant from the NKTH/ANR Neurogen (to I.U.).

1. Fox MD, Snyder AZ, Vincent JL, Raichle ME (2007) Intrinsic fluctuations within cortical systems account for intertrial variability in human behavior. *Neuron* 56:171–184.
2. Greicius M (2008) Resting-state functional connectivity in neuropsychiatric disorders. *Curr Opin Neurol* 21:424–430.
3. Hampson M, Driesen NR, Skudlarski P, Gore JC, Constable RT (2006) Brain connectivity related to working memory performance. *J Neurosci* 26:13338–13343.
4. He BJ, Shulman GL, Snyder AZ, Corbetta M (2007) The role of impaired neuronal communication in neurological disorders. *Curr Opin Neurol* 20:655–660.
5. He BJ, Snyder AZ, Zempel JM, Smyth MD, Raichle ME (2008) Electrophysiological correlates of the brain's intrinsic large-scale functional architecture. *Proc Natl Acad Sci USA* 105:16039–16044.
6. Sadaghiani S, et al. (2010) Intrinsic connectivity networks, alpha oscillations, and tonic alertness: A simultaneous electroencephalography/functional magnetic resonance imaging study. *J Neurosci* 30:10243–10250.
7. Schölvinck ML, Maier A, Ye FQ, Duyn JH, Leopold DA (2010) Neural basis of global resting-state fMRI activity. *Proc Natl Acad Sci USA* 107:10238–10243.
8. Shmuel A, Leopold DA (2008) Neuronal correlates of spontaneous fluctuations in fMRI signals in monkey visual cortex: Implications for functional connectivity at rest. *Hum Brain Mapp* 29:751–761.
9. Nir Y, et al. (2008) Interhemispheric correlations of slow spontaneous neuronal fluctuations revealed in human sensory cortex. *Nat Neurosci* 11:1100–1108.
10. Pinsk MA, Kastner S (2007) Neuroscience: Unconscious networking. *Nature* 447:46–47.
11. Lacruz ME, García Seoane JJ, Valentin A, Selway R, Alarcón G (2007) Frontal and temporal functional connections of the living human brain. *Eur J Neurosci* 26: 1357–1370.
12. Matsumoto R, et al. (2007) Functional connectivity in human cortical motor system: A cortico-cortical evoked potential study. *Brain* 130:181–197.
13. Matsumoto R, et al. (2004) Functional connectivity in the human language system: A cortico-cortical evoked potential study. *Brain* 127:2316–2330.
14. Kelly C, et al. (2010) Broca's region: Linking human brain functional connectivity data and non-human primate tracing anatomy studies. *Eur J Neurosci* 32:383–398.
15. Koyama MS, et al. (2010) Reading networks at rest. *Cereb Cortex* 20:2549–2559.
16. Biswal B, Yetkin FZ, Haughton VM, Hyde JS (1995) Functional connectivity in the motor cortex of resting human brain using echo-planar MRI. *Magn Reson Med* 34: 537–541.
17. Fox MD, Raichle ME (2007) Spontaneous fluctuations in brain activity observed with functional magnetic resonance imaging. *Nat Rev Neurosci* 8:700–711.
18. Mehta AD, Klein G (2010) Clinical utility of functional magnetic resonance imaging for brain mapping in epilepsy surgery. *Epilepsy Res* 89:126–132.
19. Fox MD, Zhang D, Snyder AZ, Raichle ME (2009) The global signal and observed anticorrelated resting state brain networks. *J Neurophysiol* 101:3270–3283.
20. Murphy K, Birn RM, Handwerker DA, Jones TB, Bandettini PA (2009) The impact of global signal regression on resting state correlations: Are anti-correlated networks introduced? *Neuroimage* 44:893–905.
21. Fox MD, et al. (2005) The human brain is intrinsically organized into dynamic, anticorrelated functional networks. *Proc Natl Acad Sci USA* 102:9673–9678.
22. Kelly AM, Uddin LQ, Biswal BB, Castellanos FX, Milham MP (2008) Competition between functional brain networks mediates behavioral variability. *Neuroimage* 39:527–537.
23. Deco G, Corbetta M (2011) The dynamical balance of the brain at rest. *Neuroscientist* 17:107–123.
24. Deco G, Jirsa VK, McIntosh AR (2011) Emerging concepts for the dynamical organization of resting-state activity in the brain. *Nat Rev Neurosci* 12:43–56.
25. Smith SM, et al. (2009) Correspondence of the brain's functional architecture during activation and rest. *Proc Natl Acad Sci USA* 106:13040–13045.
26. Margulies DS, et al. (2009) Precuneus shares intrinsic functional architecture in humans and monkeys. *Proc Natl Acad Sci USA* 106:20069–20074.
27. Nelson SM, et al. (2010) A parcellation scheme for human left lateral parietal cortex. *Neuron* 67:156–170.
28. Vincent JL, et al. (2007) Intrinsic functional architecture in the anaesthetized monkey brain. *Nature* 447:83–86.
29. Damasio H, Damasio AR (1980) The anatomical basis of conduction aphasia. *Brain* 103: 337–350.
30. Petrides M, Pandya DN (2009) Distinct parietal and temporal pathways to the homologues of Broca's area in the monkey. *PLoS Biol* 7:e1000170.
31. Cox RW (1996) AFNI: Software for analysis and visualization of functional magnetic resonance neuroimages. *Comput Biomed Res* 29:162–173.
32. Smith SM, et al. (2004) Advances in functional and structural MR image analysis and implementation as FSL. *Neuroimage* 23(Suppl 1):S208–S219.
33. Margulies DS, et al. (2007) Mapping the functional connectivity of anterior cingulate cortex. *Neuroimage* 37:579–588.
34. Johnston JM, et al. (2008) Loss of resting interhemispheric functional connectivity after complete section of the corpus callosum. *J Neurosci* 28:6453–6458.